Supporting Information for:

Solvent-Exposed Salt Bridges Influence the Kinetics of α-Helix Folding and Unfolding

Heleen Meuzelaar, Martijn Tros, Adriana Huerta-Viga, Chris N. van Dijk, Jocelyne Vreede, and Sander Woutersen*

Van 't Hoff Institute for Molecular Sciences, University of Amsterdam, Science Park 904, 1098 XH Amsterdam, The Netherlands

E-mail: S.Woutersen@uva.nl

Phone: +31 (0)20 5257091. Fax: +31 (0)20 5256456

*To whom correspondence should be addressed

Contents

1 Experimental Details

1.1 Sample preparation

The peptides ($\geq$ 95 % purity) were purchased from GL Biochem (Shanghai) and used without further purification. Residual trifluoroacetic acid (TFA) from the purification method was removed by multiple lyophilizations against a 35% DCl/D_2O solution. Stock solutions of $12-16$ mM were prepared by directly dissolving dry peptide in a 50 mM KD_2PO_4/K_2DPO_4 buffer (pH*= 7.0), resulting in peptide solutions at pH$^* = 2.5$. For measurements under neutral conditions (pH*= 7.0), the pH* value of the peptide solutions was adjusted by addition of NaOD (the volume added was less than 1% of the peptide solution).

1.2 Steady-state CD and FTIR spectroscopy

Circular dichroism (CD) spectra were collected using an Olis DSM-1000 CD Spectrophotometer equipped with a Julabo (CF31) temperature controller. All CD measurements were obtained at peptide concentrations of 40 μM in 20 mM phosphate buffer (pH= 6.8 or pH= 2.5) using 2-mm quartz cuvettes. The ellipticity is reported as mean residue ellipticity (θ), and the relative helicity in each peptide is determined by monitoring the ellipticity at 222 nm. The temperature-dependency of the ellipticity was monitored for each of the peptides between $190-257.5$ nm with incremental steps of 0.75 nm and averaging over 5 s of data acquisition time (0.15 nm/min scanning speed). The set point of the water bath is software-controlled and the actual sample temperature was continuously measured using an external temperature probe inserted into the cuvette holder. Global fitting with singular value decomposition (SVD) of the datasets collected as function of temperature were performed using the Olis GlobalWorks software package. All datasets were fitted with a two-state model ($F \rightleftharpoons U$). We find that we can describe the data by assuming no change in the specific heat upon folding ($\Delta C_p = 0$), as is to be expected since the solvent exposure does not change significantly upon helix formation.[1] The fit function used to determine ΔH_{UF} and T_m from

the SVD of the UV-CD data is given by[1]

$$\frac{[U]}{[U]+[F]} = \frac{\exp\{(-\Delta H_{\mathrm{UF}} + T\Delta S_{\mathrm{UF}})/RT\}}{1+\exp\{(-\Delta H_{\mathrm{UF}} + T\Delta S_{\mathrm{UF}})/RT\}} \tag{1}$$

where $\Delta S_{\mathrm{UF}} = \Delta H_{\mathrm{UF}}/T_{\mathrm{m}}$. To ensure a reliable estimate of the uncertainties in the values obtained from the analysis, multiple (≥ 3) datasets were acquired for each peptide, and all thermodynamic parameters (ΔH and T_{m}) derived from SVD analysis are the weighted averages of at least three measurements. The experimental errors correspond to the weighted standard error of the mean from minimal three measurements.

For the steady-state Fourier-transform infrared (FTIR) measurements we used a Bruker Vertex 70 spectrometer. The peptides were kept at $12-16$ mM concentration between 2 mm thick CaF_2 windows separated by a 50 μm Teflon spacer. Temperature control was achieved with a circulating water bath. Typically, 75 scans were signal averaged at a resolution of 2 cm^{-1} to generate one spectrum.

1.3 Molecular Dynamics Simulations

The sequence of the $(i+4)$ER peptide was modeled as an ideal α-helix using Chimera,[2] and capped with acetate at the N-terminus and methylamide at the C-terminus. Glutamate residues were deprotonated and arginine residues were protonated. This structure was solvated in a periodic dodecahedron box with a volume of 97.29 nm^3, followed by the addition of 3143 water molecules. To meet experimental conditions and ensure electrostatic neutrality of the system, 1 Na^+ ion and 1 Cl^- ion were added, representing a concentration of 20 mM NaCl. In total, the system contained 9670 atoms. Interactions between atoms were described by the AMBER99-SB force field,[3] in combination with the TIP3P water model.[4] Long-range electrostatic interactions were treated via the Particle Mesh Ewald method[5,6] with a short-range electrostatic cutoff distance at 1.1 nm. Van der Waals interactions were cut off at 1.1 nm. Preparation of the system consisted of energy minimization and 10 ps of equilibration. Energy minimization was performed by us-

ing the conjugate gradient method. After energy minimization, the positions of water molecules were equilibrated by a 10 ps molecular dynamics run at a temperature of 278 K and a pressure of 1 bar in which the heavy atoms in the protein were position-restrained with a force constant in each direction of 1000 kJ/mol nm. We performed simulations at two different temperatures: 278 K and 350 K, for each temperature three 100 ns runs. Initial conditions were varied by assigning new random starting velocities, drawn from the Maxwell-Boltzmann distribution. All simulations were performed with GROMACS v.4.5.4[7] with the leap-frog integration scheme and a time step of 2 fs, using LINCS to constrain bonds in the protein and SETTLE to constrain water bonds. All simulations were performed in the isothermal-isobaric ensemble at a pressure of 1 bar, using the v-rescale thermostat[8] and the Parrinello-Rahman barostat.[9]

Frames were stored every 5 ps. Analysis consisted of counting the number of helical hydrogen bonds, indicated as *hhb*, and counting the number of salt bridges occurring within a repeat, indicated as *nsb*. Helical hydrogen bonds were defined as the hydrogen bond between the backbone carbonyl oxygen of residue i and the backbone amide nitrogen of residue $i+4$. A helical hydrogen bond was counted if the distance between these atoms was less then 0.35 nm and the angle between oxygen, nitrogen and hydrogen was less than 30^o. A salt bridge was counted if it occurred between the glutamate and arginine within the same repeat and with a distance between the Glu-C_δ and Arg-C_ζ atom less than 0.8 nm. Excluding the first 10 ns of each simulation, two-dimensional probability distributions were calculated of *hhb* and *nsb*, with a binsize of 1, and contoured at intervals of 1 %. Snapshots were visualized with VMD.[10]

1.4 Time-resolved T-jump IR experiments

Laser-induced T-jumps of 6 to 8 K were obtained by nanosecond excitation of the OD-stretch overtone of D_2O using the same optical setup as described previously.[11] In brief, the T-jump pulse is generated using a beta barium borate (BBO)-based optical parametric oscillator (OPO) pumped by the second harmonic (λ = 532 nm) of a 20-Hz, Q-switched Nd:YAG laser (Quanta-

Ray INDI, Spectra-Physics). The idler pulse (λ =1.98 μm, 12.5 mJ, 5 ns FWHM) is focused (f = 75 mm, CaF_2) to 500 μm diameter at the sample, leading to a temperature-rise within the pulse width of the laser. The temperature-induced absorption changes induced in the sample are detected at various time delays after the T-jump by mid-infrared (mid-IR) probe pulses using the 800 nm output of a commercial Ti:sapphire laser (Spectra-Physics Hurricane, 1 kHz, 1 mJ, 100 fs FWHM) to pump a BBO based optical parametric amplifier (OPA). Subsequent difference-frequency generation of signal and idler in $AgGaS_2$ results in mid-IR pulses with a duration of $\sim$150 fs centered at 1620 cm^{-1}, and with a FWHM bandwidth of 200 cm^{-1}, and an energy of 1 μJ. The mid-IR pulse is split into probe and reference pulses by means of a 50/50 beamsplitter, which are subsequently focused through the sample by means of a 100 mm off-axis parabolic mirror. Synchronization between the T-jump pulse and the mid-IR probe pulses is based on the electronic configuration described elsewhere.[12]

To obtain transient IR spectra, we determine absorption changes $\Delta A = A - A_0 = -\log_{10}(T/T_0)$, where T and T_0 are the transmission of the IR-probe pulse in the presence and absence of the T-jump pulse, respectively, as described previously.[12] We correct for small pulse-to-pulse fluctuations in the intensity of the IR-probe pulses by simultaneously measuring the intensity of a reference pulse (split off from the probe pulse before the sample) that passes through the sample in an area that is not influenced by the T-jump pulse. Transient absorption changes are measured using frequency-dispersed detection of the probe and reference pulses using a liquid-nitrogen-cooled 2$\times$32 HgCdTe (MCT) array detector (Infrared Associates).

Each delay value is the average of approximately 1000 T-jumps. Given the repetition frequency of the T-jump laser (20 Hz), care is taken to ensure that the sample has relaxed back to its initial temperature before the subsequent T-jump. The initial temperature of the sample was controlled using a thermostatted cell-holder with a circulating heat bath and was calibrated with an IR camera (FLIR ThermaCAM E2). Reference samples containing the D_2O buffer solution were measured under identical conditions and used to correct for contributions of the solvent to the transient signals. The transient absorbance change of the D_2O buffer solution also provides

information about the magnitude of the *T*-jump, and was used to calibrate the size of the *T*-jump using the steady-state absorbance change of the buffer with temperature (which are only due to changes in D_2O). The IR response of D_2O can be used as an internal thermometer due to its nearly linear response with temperature in the amide I' spectral region.[13]

2 Additional Data

2.1 Temperature-dependent UV-CD measurements

The helix-coil transition of the peptides was analyzed in thermal equilibrium using CD spectroscopy. UV CD spectra were collected between 190−257.5 nm in a temperature range of 260−346 K under both neutral and acidic pH conditions (Fig. 1). The dependence on temperature of the mean residue ellipticity detected at 222 nm for each of the peptides at neutral and acidic pH is shown in Fig. 2. The thermal unfolding curves have a sigmoidal shape, and from a singular value decomposition of the temperature-dependent CD spectra and global fitting we find that the folding is well described by a two-state model. The melting temperatures T_{m} and the unfolding enthalpy changes ΔH are listed in Table 1. The observed helicity and thermodynamic stability obtained at neutral pH (Fig. 2a) follows the trend $(i+4)\mathrm{ER} > (i+3)\mathrm{ER} \approx (i+4)\mathrm{RE} > (i+3)\mathrm{RE}$, indicating that the α-helix-stabilizing effect is largest for ER-oriented salt bridges in which E and R are spaced four peptide units apart, as was reported previously.[14]

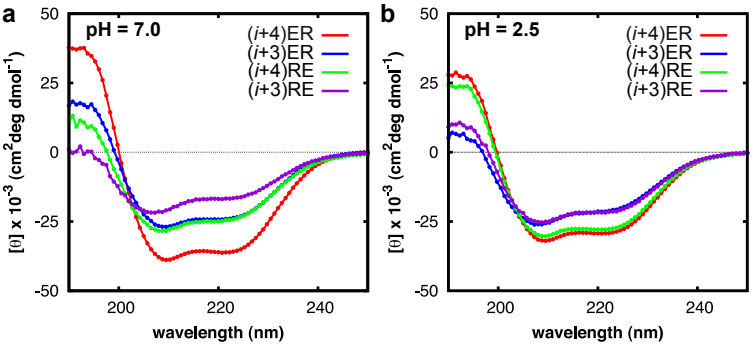

Figure 1: Far-UV circular dichroism spectra of the different ER and RE peptides measured at 274 K at (a) neutral and (b) acidic pH.

To confirm that the salt bridges provide (de)stabilization to the α-helical structure, the salt-bridge formation was inhibited by protonating the Glu side-chains at acidic pH (Fig. 2b). Under these conditions, the relative helicity and stability of the peptides is $(i+4)\mathrm{ER} \approx (i+4)\mathrm{RE} > (i+3)\mathrm{ER} \approx (i+3)\mathrm{RE}$, which agrees with previously reported results.[14] The dichotomy observed between the $(i,i+4)$ and $(i,i+3)$ spaced peptides in absence of salt bridges probably arises from

the fact that the helix-forming propensity of amino acids may depend slightly on their position in the sequence of a peptide. Comparison of the melting curves at neutral and acidic pH (Fig. 2a and b) shows that the relative α-helix content and thermodynamic stability of the ER-type peptides decrease due to disruption of the favorable salt-bridge interaction at acidic pH. In contrast, the RE-oriented peptides show an enhanced helicity and stability in the absence of salt-bridge interactions, indicating that the formation of RE-oriented salt bridges at neutral pH *destabilize* the α-helical conformation. The observed differences in thermodynamic stability of the investigated peptides at neutral pH probably arise mainly from intrinsically preferred rotameric states of Glu and Arg side chains when these residues are in an α-helix.[15–20]

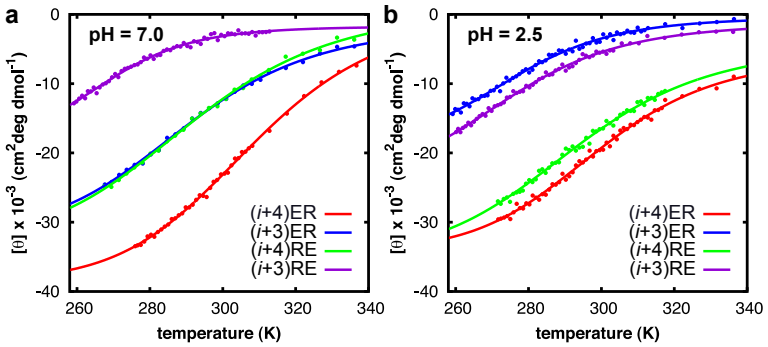

Figure 2: Temperature-dependency of the mean residue ellipticity at 222 nm (θ_{222}) of each of the four peptides at (a) neutral and (b) acidic pH. The curves represent a least-square fit to a two-state model.[1]

Table 1: Thermodynamic parameters ($\Delta H_{UF} = H_U - H_F$, and T_m) derived from SVD and global fitting analysis of the temperature-dependent UV CD data of the peptides at neutral and acidic pH.

	ΔH_{UF} (kJ mol^{-1})	T_m (K)	ΔH_{UF} (kJ mol^{-1})	T_m (K)
Peptide	pH = 7.0 **(with salt bridge)**		pH = 2.5 **(no salt bridge)**	
$(i+4)$ER	40.2 ± 1.6	312.9 ± 1.2	41.8 ± 2.4	295.7 ± 1.4
$(i+3)$ER	41.0 ± 4.1	289.1 ± 1.1	36.5 ± 1.9	275.4 ± 2.5
$(i+4)$RE	47.4 ± 1.5	290.0 ± 1.2	47.4 ± 2.5	294.1 ± 3.2
$(i+3)$RE	51.9 ± 5.9	270.0 ± 2.3	36.9 ± 3.4	272.6 ± 0.7

All values shown are the weighted average of at least three measurements. The corresponding errors indicate the weighted standard error of the mean from minimal three measurements.

2.2 Unfolding in thermal equilibrium monitored by UV-CD and FTIR spectroscopy

In Fig. 3 we compare the temperature-dependency of the mean residue ellipticity at 222 nm monitored using UV-CD and the temperature-dependent FTIR response at 1630 cm^{-1} (decrease of the α-helical population, (a)) and 1658 cm^{-1} (increase of the random coil population, (b)) of peptide $(i+4)$ER at neutral pH. Both the UV-CD and FTIR thermal unfolding curves show a sigmoidal transition, reflecting the temperature-induced conformational changes of the peptide in thermal equilibrium. From least-squares fits of the temperature-dependent FTIR data at both frequencies to a two-state model,[1] we obtain a melting temperature T_m of 310.5 $\pm$ 2.5 K, which is in quantitative agreement with the thermal melting point of 312.9 $\pm$ 1.2 K (see Table 1) obtained from SVD and global fitting analysis of the temperature-dependent CD data. Therefore, our static temperature-dependent CD and IR data further support that the thermal unfolding of this peptide can be described by an effective two-state model.

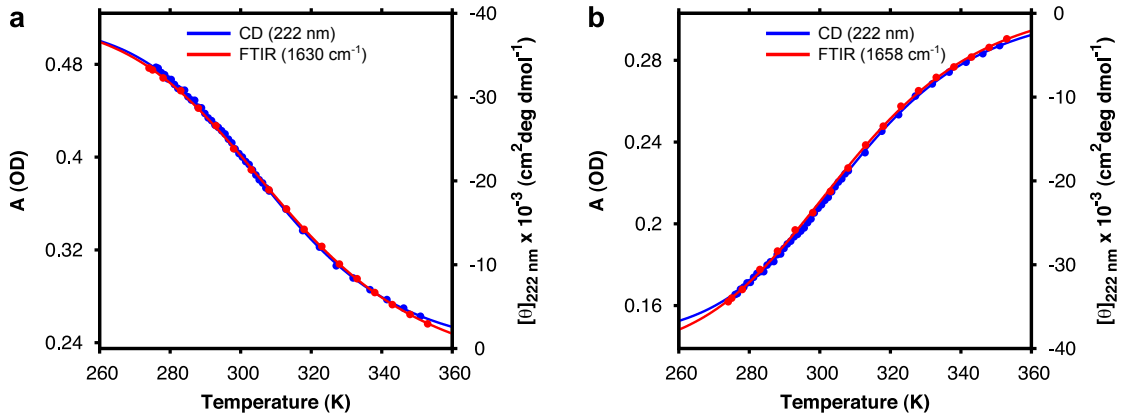

Figure 3: Thermal melting curves of peptide $(i+4)$ER at neutral pH detected at 222 nm (θ_{222}) using UV-CD (blue), and FTIR spectroscopy (red) at (a) 1630 cm^{-1} (decrease of the α-helical population) and (b) 1658 cm^{-1} (increase of the random coil population). The solid curves represent least-square fits to a two-state model.[1] In order to compare the UV-CD melting curve with the temperature-dependent FTIR response detected at 1658 cm^{-1}, the y-axis representing the θ_{222} response in (b) is reversed compared to (a).

2.3 Effect of intrinsically preferred side-chain rotamers on folding thermodynamics

The differences in thermodynamic stability (the free-energy difference ΔG_{UF} between the unfolded and folded states) of the four investigated peptides are in agreement with previous results,[14] and probably arise mostly from sterical effects. The preferred Glu and Arg rotameric states (which depend on the backbone conformation) may allow salt-bridge formation in one orientation of Glu and Arg, but not in the other, causing a difference in the helix stability of the peptides with ER and RE oriented residues. To gain more insight into the effect of rotameric states on the thermodynamic stability of the investigated peptides, we determine the number and relative probability of the accessible side-chain χ rotamers that allow the formation of Glu$-$Arg salt bridges using Richardson's rotamer library[21] implemented in Chimera.[22] For this purpose, we have performed a systematic search to determine which intrinsically preferred side-chain conformations (χ angles) of Glu and Arg in an α-helical backbone conformation are such that salt-bridge formation is possible, i.e., are such that the distance between at least one Glu oxygen and one Arg nitrogen atom is between 2.70 and 3.00 Å. The center value of this distance range was chosen based on X-ray measurements on a $\mathrm{Glu}^{-}-\mathrm{Arg}^{+}$ model compound, from which it was found that the distances between the oxygen and nitrogen atoms of the two $\mathrm{Glu}^{-}-\mathrm{Arg}^{+}$ hydrogen bonds in an optimal salt bridge are 2.81 Å and 2.89 Å.[23,24] Sterically forbidden conformations were excluded, and only rotameric states with probability $\geq 0.5\%$ were taken into account.

For the α-helical backbone conformation of peptide $(i+4)$ER we find three different accessible rotameric isomers in which the relative orientation of the intrinsically preferred side-chain conformations of Glu and Arg is such that salt-bridge formation is possible (Fig. S6). For the α-helical backbone conformation of the thermodynamically less stable peptides $(i+3)$ER, $(i+4)$RE, and $(i+3)$RE, no (sterically unhindered) rotameric states that allow the formation of a salt bridge are significantly populated according to the rotameric library,[21] suggesting that the formation of salt bridges in the folded states of these peptides requires deviation of the χ angles from their intrinsically preferred χ angles, and/or of the backbone ϕ, ψ angles from their ideal α-helical values. In

either case, the helix-stabilizing effect of the salt bridges will be less. Thus, the observed differences in thermal stability between the different peptides probably originate from differences in their geometric ability to form (intrinsically preferred) low-energy side-chain rotamers that allow salt-bridge formation. In addition, the salt-bridging residue pairs in the folded state of peptide $(i+4)$ER possibly enjoy a larger degree of freedom due to the ability to occupy multiple intrinsically preferred salt-bridging Glu−Arg rotamer pairs, and contributes entropically to the free-energy balance of the peptide.[16,19]

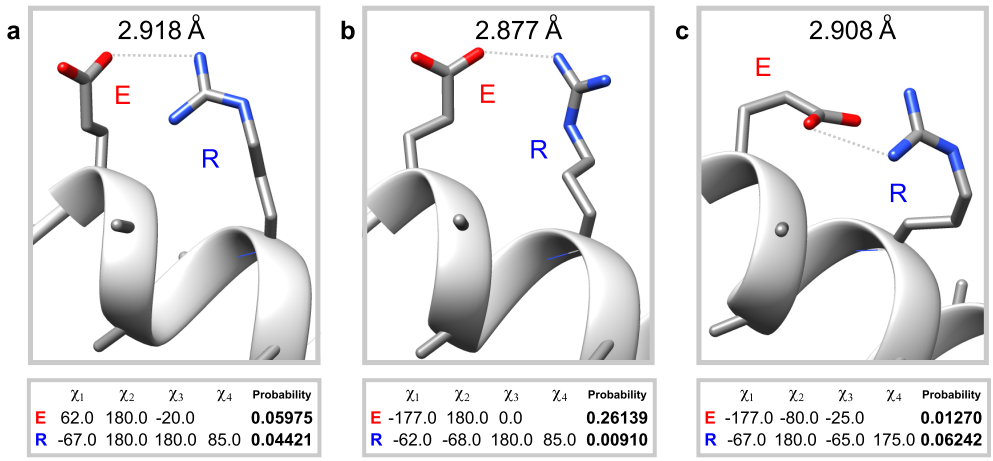

	χ_1	χ_2	χ_3	χ_4	Probability
E	62.0	180.0	-20.0		**0.05975**
R	-67.0	180.0	180.0	85.0	**0.04421**

	χ_1	χ_2	χ_3	χ_4	Probability
E	-177.0	180.0	0.0		**0.26139**
R	-62.0	-68.0	180.0	85.0	**0.00910**

	χ_1	χ_2	χ_3	χ_4	Probability
E	-177.0	-80.0	-25.0		**0.01270**
R	-67.0	180.0	-65.0	175.0	**0.06242**

Figure 4: Representation of the rotameric isomers of peptide $(i+4)$ER in which the geometrical orientation of the intrinsically preferred rotamer conformations of side-chains Glu (E) and Arg (R) are such that salt-bridge formation is possible. The distance between the oxygen and nitrogen atoms of the Glu−Arg rotamer pairs are (a) 2.918, (b) 2.877, and (c) 2.908 Å. The local backbone is cartooned. The corresponding rotamer torsion angles (χ_1, χ_2, χ_3, and χ_4) and library probability values are estimated using Richardson's rotamer library[21] and refer to the intrinsic backbone-dependent side-chain rotamer preference of Glu (E) and Arg (R). Pictures rendered with Chimera.[22]

2.4 MD results confirming salt-bridge breaking upon thermal unfolding

To obtain detailed insights into the folded and unfolded conformations, we performed Molecular Dynamics simulations of peptide $(i+4)$ER at two different temperatures, 278 K and 350 K. At lower temperature, the peptide would be fully folded, whereas it would be completely unfolded at the higher temperature. Sampling consisted of three independent 100 ns runs for each temperature. Loss of helical structure can be characterized by a drop in the number of helical hydrogen bonds *hhb*. A helical hydrogen bond occurs if the carbonyl oxygen of residue i and the amide nitrogen in residue $i+4$ are less than 0.35 nm apart, and the O-N-H angle is less than 30 degrees. If the entire $(i+4)$ER peptide is in a perfectly helical conformation, *hhb* is equal to 15, including the terminal caps. The presence of salt bridges is indicated by *nsb*, the number of salt bridges. If the distance between atoms C_ζ of arginine and C_δ of glutamate is less than 0.8 nm, and if the arginine and glutamate are within the same repeat, a salt bridge is counted. The maximum value of *nsb* is 3. Fig. 5 (a) and (b) shows two-dimensional probability distributions as a function of *hhb* and *nsb*. At 278 K the distribution peaks at (*hhb*, *nsb*) = (6, 2), whereas the peak for 350 K has shifted to lower values at (*hhb*, *nsb*) = (0, 0). The peptides at 278 K have more helical character and exhibit more salt bridges than at 350 K. However, not all salt bridges are lost at 350 K. Time traces of the salt bridge distances d_{sb} show that salt bridges form and break in all three repeats (see Fig. 5 (c) and (d)). We find that both the α-helical conformation and native Glu$-$Arg salt bridges are highly populated at low temperature (the distribution peaks at $nsb = 2$). On the other hand, at high temperature both the α-helical structure and Glu$-$Arg interactions are hardly populated (*nsb* peaks at ≈ 0). We therefore conclude that the salt bridges indeed break upon thermal unfolding. Fig. 5 (e) and (f) show typical snapshots, taken from the peaks in the probability distributions.

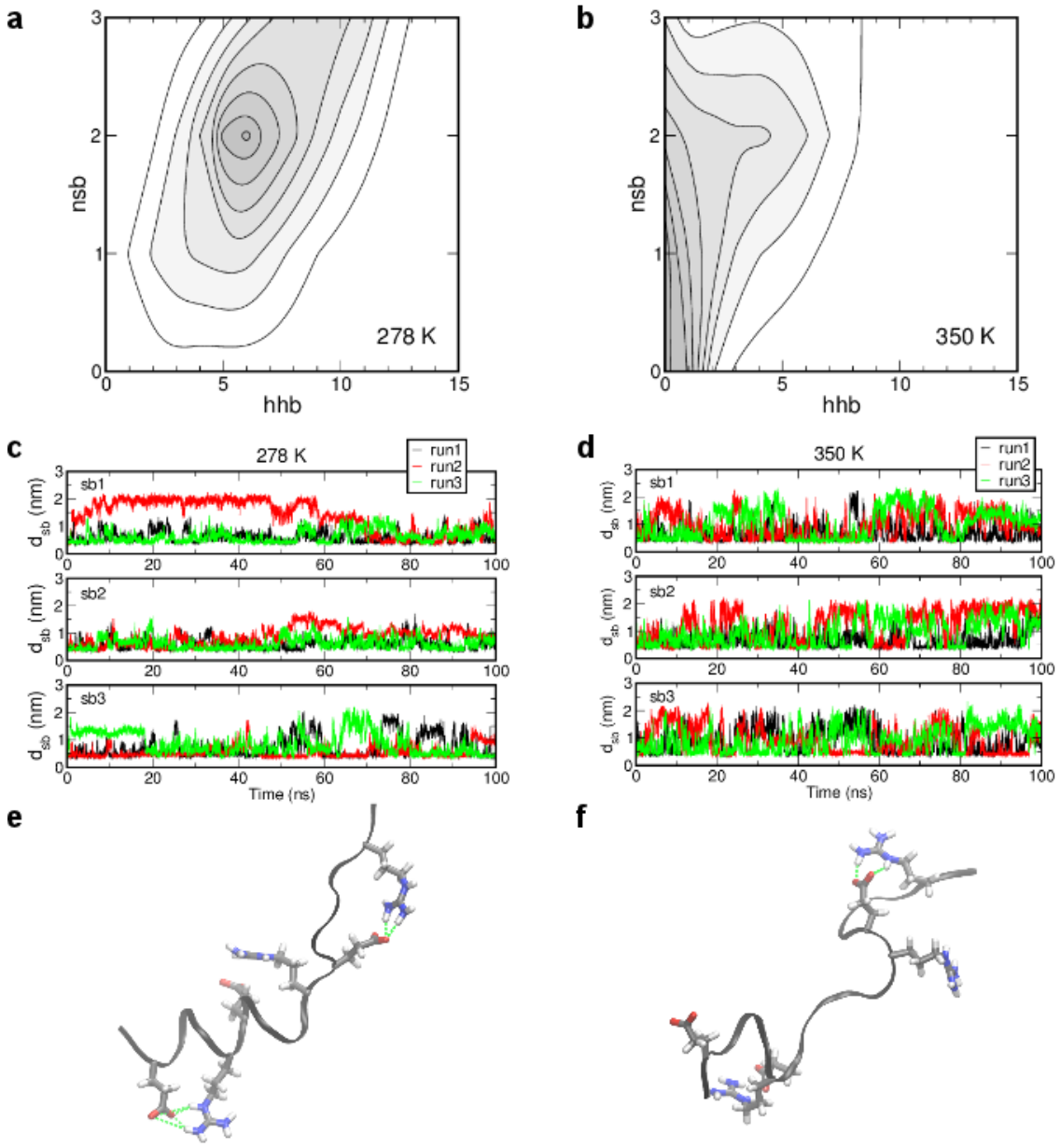

Figure 5: (a), (b) two-dimensional probability plots as a function of the number of helical hydrogen bonds *hhb* and number of in-repeat salt bridges *nsb* at (a) 278 K and (b) 350 K. Contour lines are drawn at intervals of 0.01. Darker grey indicates a higher population. (c), (d) Time traces of salt bridge distances d_{sb} in the three repeats at (c) 278 K and (d) 350 K. Each run is displayed in a different color. The labels starting with sb indicate the repeat in which the salt bridge is located. (e), (f) Representative snapshots of the conformations at (e) 278 K and (f) 350 K, taken from the peaks in the probability distributions. The backbone of the peptide is drawn as a grey ribbon. The side chains of the arginine and glutamate residues are shown as sticks with the following color code: grey - carbon, red - oxygen, blue - nitrogen, white - hydrogen. The green dashed lines indicate a formed salt bridge.

2.5 T-jump control measurements

To verify that the origin of the kinetic phase arises from the folding/unfolding re-equilibration of the peptides, we measure the transient absorption changes of an aqueous solution of N-methylacetamide (NMA, which contains a single trans-peptide group) in response to a nanosecond T-jump (Fig. 6). As can be seen in Fig. 6b, the transient absorption changes of NMA shows an instantaneous T-jump response, which is very similar to the instantaneous response as observed for the different peptides (see Fig. 2). However, the T-jump relaxation of NMA does not exhibit a kinetic phase, and we conclude that the observed kinetic phase as observed for the peptides arises from the conformational redistribution process of the peptides during re-equilibration.

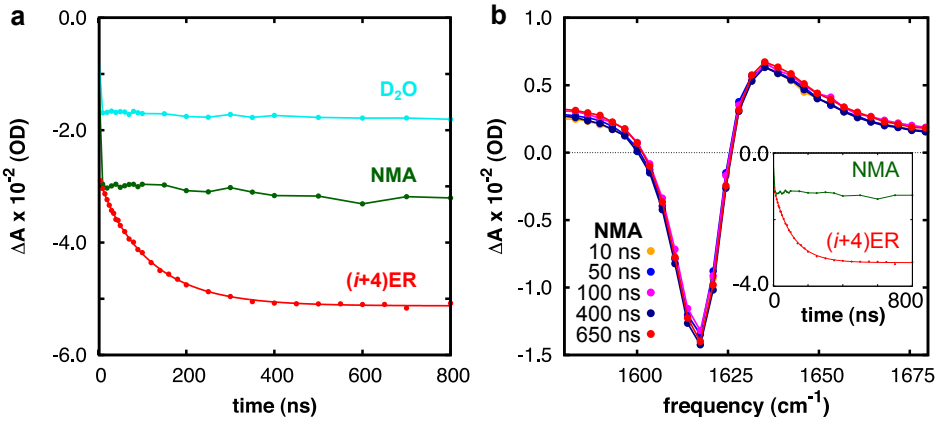

Figure 6: (a) Transient absorption changes (uncorrected for solvent contributions) of N-methylacetamide (NMA), D_2O, and peptide $(i+4)$ER following a T-jump from 301 to 307 K monitored at 1630 cm^{-1}. (b) Solvent-corrected transient spectra of NMA obtained at several time delays after the T-jump pulse ($\Delta T = 6$ K). The connecting lines are a guide to the eye. The inset compares the D_2O-corrected T-jump relaxation of NMA and peptide $(i+4)$ER monitored at 1630 cm^{-1}.

2.6 Infrared spectrum as a probe of the Glu protonation state

To probe the α-helix content we examine the IR response of the peptides, see Fig. 7. The amide I' absorbance of proteins and peptides, mainly originating from backbone C=O stretch vibrations, is a sensitive probe of secondary structure and can be directly related to the backbone conformation.[25] In particular, amide residues in an α-helix absorb at $\sim$1635 cm^{-1}, whereas those in a random coil absorb at 1645 cm^{-1}.[26] The differences in helicity between the four peptides as derived from the amide I' maximum in the low-temperature equilibrium FTIR spectra (Fig. 7) are in agreement with those derived from the CD results (see Fig. 1). The smaller peaks at 1585 and 1607 cm^{-1} originate from the symmetric and antisymmetric stretch vibration of the guanidinium ($CN_3H_5^+$) group of Arg^+.[26] The band observed at 1565 cm^{-1} in the FTIR spectra at neutral pH arises from the CO-stretching mode of the COO^- group of Glu^- (Fig. 7a), and shifts to 1705 cm^{-1} upon protonation[26] (Fig. 7b). The absence of the COO^- peak at pH = 2.5 confirms that the carboxylate groups of the Glu side chains are completely protonated at this pH, making salt-bridge formation impossible.

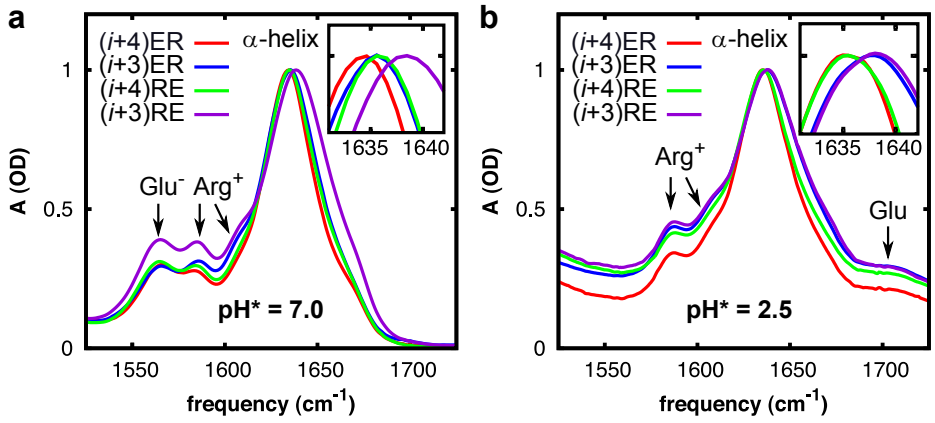

Figure 7: Normalized low-temperature equilibrium FTIR spectra in the amide I' region of each of the peptides obtained at 278 K under (a) neutral and (b) acidic pH conditions. The spectral feature arising from the ν_{as}(C=O) mode of the COO^- group of Glu^- observed at 1565 cm^{-1} in the FTIR spectra at neutral pH (a) shifts to higher frequency upon protonation and appears at 1705 cm^{-1} (the ν(C=O) mode of the Glu COOH group)[26] in the FTIR spectra obtained under acidic pH conditions (pH* = 2.5). This unambiguously demonstrates that salt-bridge formation at a pH value of 2.5 is prevented due to protonation of the carboxylate groups of Glu. The insets compare the amide I' center frequencies.

2.7 Two-state folding behavior at all temperatures, pH values, and IR frequencies

The T-jump-induced re-equilibration between α-helical and random coil ensembles was probed at a wide range of temperatures in the amide I' spectral region. As can be seen in Fig. 8, all transients show single-exponential T-jump relaxation kinetics. The detection of single-exponential T-jump relaxation kinetics with equal relaxation rates observed at 1630 cm^{-1} and 1658 cm^{-1} at all final T-jump temperatures and at both the investigated pH values indicates that the dynamics of the helix-coil transition can be described by an effective two-state model,[27,28] and that the α-helical and random-coil state ensembles can be described as two broad free-energy minima in the conformational free-energy landscape, which are separated by a single kinetic barrier.[29–31] This is in agreement with previous studies that showed that the *ensemble* dynamics of the helix-coil transition can be well approximated using two-state analysis.[29–37]

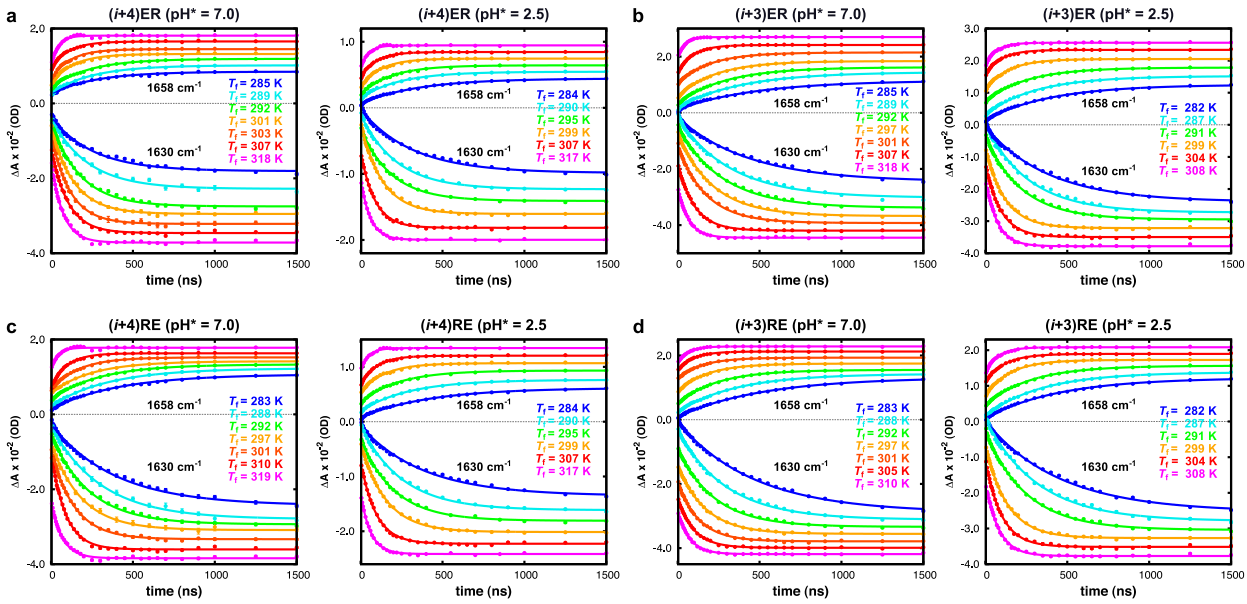

Figure 8: Solvent-corrected relaxation kinetics monitored at 1630 cm^{-1} (α-helix), and 1658 cm^{-1} (random coil) of peptides (a) $(i+4)$ER, (b) $(i+3)$ER, (c) $(i+4)$RE, and (d) $(i+3)$RE measured at different final T-jump temperatures at neutral and acidic pH. The relaxation kinetics are globally fitted to a single-exponential decay function (solid curve): $\Delta A(t) = A_0 + A_1 \exp(-t/\tau)$. The temperature values (T_f) refer to the final T-jump temperatures at the new thermal equilibrium conditions.

2.8 Complete data set underlying Figures 5 and 6 of article

We find that the effective folding and unfolding rates ($k_{\mathrm{F,eff}}$ and $k_{\mathrm{U,eff}}$) of each of the peptides exhibit Eyring temperature-dependence, and from least-squares fits of the data to the Eyring equation we obtain the effective transition enthalpy ($\Delta H^{\ddagger}_{\mathrm{eff}}$) and entropy ($\Delta S^{\ddagger}_{\mathrm{eff}}$), both for the folding (U $\rightarrow$ F) and unfolding (F $\rightarrow$ U) transitions. The results are listed in Table 1 (folding) and Table 2 (unfolding).

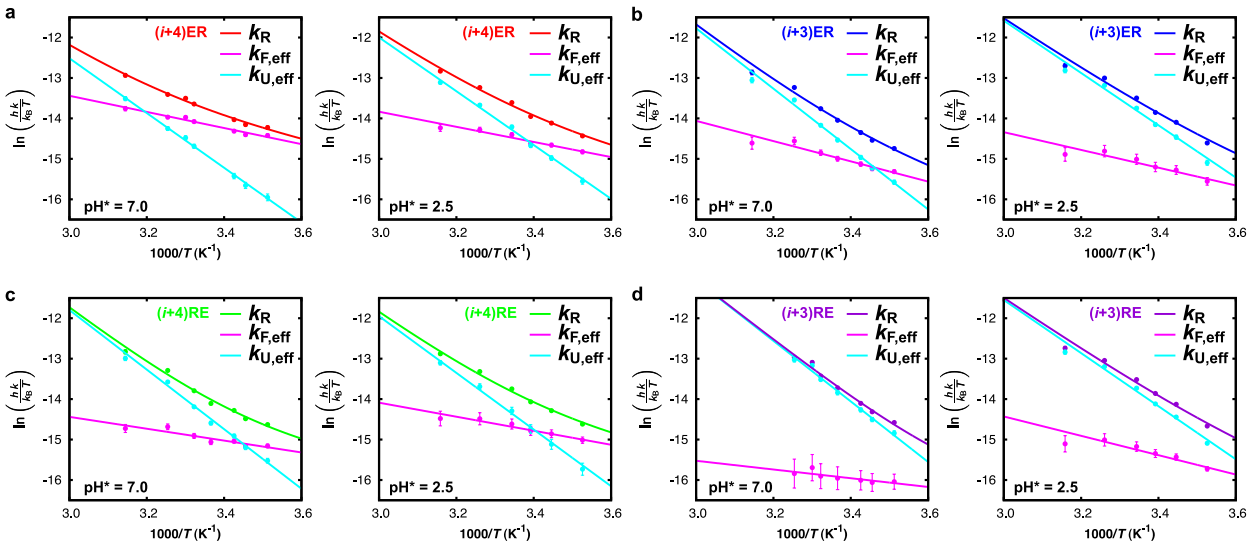

Figure 9: Eyring plots of the rate constants of the peptide (a) $(i+4)$ER, (b) $(i+3)$ER, (c) $(i+4)$RE, and (d) $(i+3)$RE, measured at neutral and acidic pH. The effective folding and unfolding rate constants ($k_{\mathrm{F,eff}}$ and $k_{\mathrm{U,eff}}$) were obtained from the T-jump relaxation rates (k_{R}) and the folding equilibrium constants (K_{eq}) according to a two-state analysis. The straight lines are linear fits.

2.9 Correlation between free-energy barriers and equilibrium free-energy difference

We find a correlation between the equilibrium free-energy difference (ΔG_{UF}) and the free-energy barriers for the folding and unfolding processes ($\Delta G^{\ddagger}_{\mathrm{U}\to\mathrm{F}}$ and $\Delta G^{\ddagger}_{\mathrm{F}\to\mathrm{U}}$, respectively), see the Figure below.

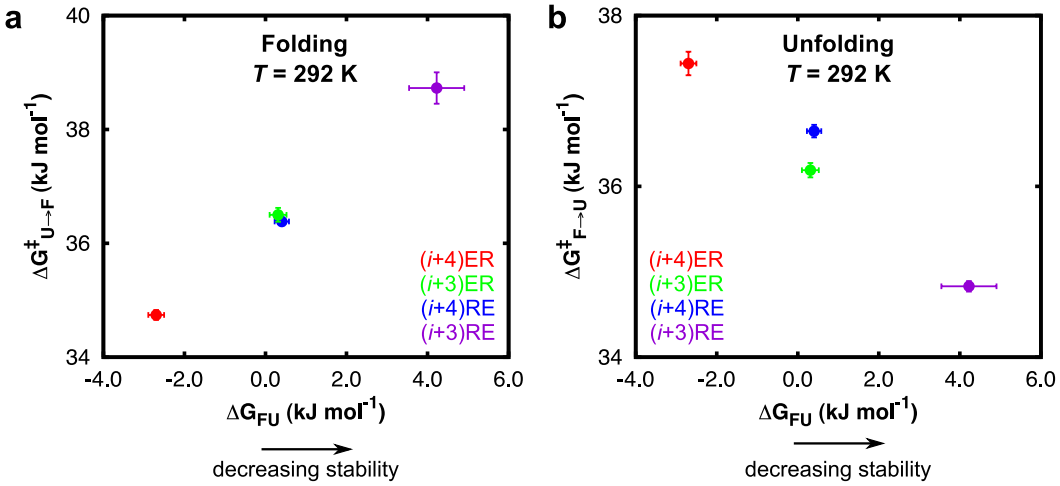

Figure 10: The transition-state barriers as a function of the free-energy difference between the folded and unfolded state ($\Delta G_{\mathrm{FU}} = G_{\mathrm{F}} - G_{\mathrm{U}}$) at 292 K for the different peptides at neutral pH. There is a clear correlation between the thermodynamic stability of the native structure and the (a) folding rates ($\Delta G^{\ddagger}{}_{\mathrm{U}\to\mathrm{F}}$) and the (b) unfolding rates ($\Delta G^{\ddagger}{}_{\mathrm{F}\to\mathrm{U}}$).

Table 2: Experimentally obtained values for $\Delta H^{\ddagger}_{\mathrm{app}}$ and $\Delta S^{\ddagger}_{\mathrm{app}}$ for the unfolding (F $\to$ U) transitions of the four investigated peptides obtained at neutral pH and at acidic pH.

	$\Delta H^{\ddagger}_{\mathrm{app\ (U\to F)}}$ (kJ mol^{-1})	$\Delta S^{\ddagger}_{\mathrm{app\ (U\to F)}}$ (J mol^{-1} K^{-1})	$\Delta H^{\ddagger}_{\mathrm{app\ (U\to F)}}$ (kJ mol^{-1})	$\Delta S^{\ddagger}_{\mathrm{app\ (U\to F)}}$ (J mol^{-1} K^{-1})
Peptide	pH = 7.0 **(with salt bridge)**		pH = 2.5 **(no salt bridge)**	
$(i+4)$ER	56.3 ± 1.7	64.9 ± 5.4	55.3 ± 1.4	66.0 ± 4.5
$(i+3)$ER	62.4 ± 0.8	87.7 ± 2.7	54.3 ± 1.0	66.1 ± 3.4
$(i+4)$RE	60.8 ± 1.3	84.0 ± 4.3	58.3 ± 2.4	75.6 ± 7.8
$(i+3)$RE	57.8 ± 0.8	78.2 ± 2.6	53.6 ± 0.7	63.4 ± 2.3

References

(1) Fersht, A. *Structure and Mechanism in Protein Science*; Freeman & Co.: New York, 1999.

(2) Pettersen, E.; Goddard, T.; Huang, C.; Couch,; G.S.,; Greenblatt, D.; Meng, E.; Ferrin, T. UCSF Chimera - A Visualization System for Exploratory Research and Analysis. *J. Comput. Chem.* **2004**, *25*, 1605–1612.

(3) Hornak, V.; Abel, R.; Okur, A.; Strockbine, B.; Roitberg, A.; Simmerling, C. Comparison of Multiple Amber Force Fields and Development of Improved Protein Backbone Parameters. *Proteins: Struct. Funct. Gen.* **2006**, *65*, 712–725.

(4) Jorgensen, W. L.; Chandrasekhar, J.; Madura, J. D.; Impey, R. W.; Klein, M. L. Comparison of Simple Potential Functions for Simulating Liquid Water. *J. Chem. Phys.* **1983**, *79*, 926–935.

(5) Darden, T.; York, D.; Pedersen, L. Particle Mesh Ewald - An N Log(N) Method for Ewals Sums in Large Systems. *J. Chem. Phys.* **1993**, *98*, 10089–10092.

(6) Essmann, U.; Perera, L.; Berkowitz, M. L.; Darden, T.; Lee, H.; Pedersen, L. G. A Smooth Particle Mesh Ewald Method. *J. Chem. Phys.* **1995**, *103*, 8577–8593.

(7) Pronk, S.; Páll, S.; Schulz, R.; Larsson, P.; Bjelkmar, P.; Apostolov, R.; Shirts, M.; Smith, J.; Kasson, P.; van der Spoel, D. et al. GROMACS 4.5: A High-Throughput and Highly Parallel Open Source Molecular Simulation Toolkit. *Bioinformatics* **2013**, *29*, 845–854.

(8) Bussi, G.; Donadio, D.; Parrinello, M. Canonical Sampling Through Velocity Rescaling. *J. Chem. Phys.* **2007**, *126*, 014101.

(9) Parrinello, M.; Rahman, A. Polymorphic Transitions in Single Crystals: A New Molecular Dynamics Method. *J. Appl. Phys.* **1981**, *52*, 7182–7190.

(10) Humphrey, W.; Dalke, A.; Schulten, K. VMD - Visual Molecular Dynamics. *J. Mol. Graphics* **1996**, *14*, 33–38.

(11) Meuzelaar, H.; Marino, K. A.; Huerta-Viga, A.; Panman, M. R.; Smeenk, L. E. J.; Kettelarij, A. J.; van Maarseveen, J. H.; Timmerman, P.; Bolhuis, P. G.; Woutersen, S. Folding Dynamics of the Trp-Cage Miniprotein: Evidence for a Native-Like Intermediate from Combined Time-Resolved Vibrational Spectroscopy and Molecular Dynamics Simulations. *J. Phys. Chem. B* **2013**, *117*, 11490–11501.

(12) Panman, M. R.; Bodis, P.; Shaw, D. J.; Bakker, B. H.; Newton, A. C.; Kay, E. R.; Leigh, D. A.; Buma, W. J.; Brouwer, A. M.; Woutersen, S. Time-resolved Vibrational Spectroscopy of a Molecular Shuttle. *Phys. Chem. Chem. Phys.* **2012**, *14*, 1865–1875.

(13) Williams, S.; Causgrove, T. P.; Gilmanshin, R.; Fang, K. S.; Callender, R. H.; Woodruff, W. H.; Dyer, R. B. Fast Events in Protein Folding: Helix Melting and Formation in a Small Peptide. *Biochemistry* **1996**, *35*, 691–697.

(14) Huyghues-Despointes, B. M. P.; Scholtz, J. M.; Baldwin, R. L. Helical Peptides with Three Pairs of Asp-Arg and Glu-Arg Residues in Different Orientations and Spacings. *Protein Sci* **1993**, *2*, 80–85.

(15) Dunbrack, R. L.; Karplus, M. Conformational-Analysis of the Backbone-Dependent Rotamer Preferences of Protein Side-Chains. *Nat. Struct. Biol.* **1994**, *1*, 334–340.

(16) Doig, A. J.; Sternberg, M. J. E. Side-Chain Conformational Entropy In Protein-Folding. *Protein Sci* **1995**, *4*, 2247–2251.

(17) Stapley, B. J.; Doig, A. J. Free Energies of Amino Acid Side-Chain Rotamers in α-Helices, β-Sheets and α-Helix N-Caps. *J. Mol. Biol.* **1997**, *272*, 456–464.

(18) Penel, S.; Doig, A. J. Rotamer Strain Energy in Protein Helices - Quantification of a Major Force Opposing Protein Folding. *J. Mol. Biol.* **2001**, *305*, 961–968.

(19) Berezovsky, I. N.; Zeldovich, K. B.; Shakhnovich, E. I. Positive and Negative Design in Stability and Thermal Adaptation of Natural Proteins. *PLoS Comput. Biol.* **2007**, *3*, e52.

(20) Donald, J. E.; Kulp, D. W.; DeGrado, W. F. Salt bridges: Geometrically Specific, Designable Interactions. *Proteins* **2011**, *79*, 898–915.

(21) Lovell, S. C.; Word, J. M.; Richardson, J. S.; Richardson, D. C. The Penultimate Rotamer Library. *Proteins* **2000**, *40*, 389–408.

(22) Pettersen, E. F.; Goddard, T. D.; Huang, C. C.; Couch, G. S.; Greenblatt, D. M.; Meng, E. C.; Ferrin, T. E. UCSF Chimera - A Visualization System for Exploratory Research and Analysis. *J. Comput. Chem.* **2004**, *25*, 1605–1612.

(23) Bray, D.; Slattery, N.; Russell, C. Guanidinium-Carboxylate Interaction: Methylguanidinium Formate. *Int. J. Pept. Prot. Res.* **1984**, *24*, 414–418.

(24) Creighton, T. E. *Proteins Structures and Molecular Properties*; Freeman, New York, 1993.

(25) Krimm, S.; Bandekar, J. Vibrational Spectroscopy and Conformation of Peptides, Polypeptides, and Proteins. *Adv. Protein Chem.* **1986**, *38*, 181–364.

(26) Barth, A.; Zscherp, C. What Vibrations Tell About Proteins. *Q. Rev. Biophys.* **2002**, *35*, 369–430.

(27) Zwanzig, R. Two-state Models of Protein Folding Kinetics. *Proc. Natl. Acad. Sci. U.S.A.* **1997**, *94*, 148–150.

(28) Nölting, B. *Protein Folding Kinetics*; Springer Berlin / Heidelberg / New York, 2006.

(29) Werner, J. H.; Dyer, R. B.; Fesinmeyer, R. M.; Andersen, N. H. Dynamics of the Primary Processes of Protein Folding: Helix Nucleation. *J. Phys. Chem. B* **2001**, *106*, 487–494.

(30) Wang, T.; Du, D.; Gai, F. Helix−Coil Kinetics of Two 14-Residue Peptides. *Chem. Phys. Lett.* **2003**, *370*, 842–848.

(31) Huang, C. Y.; He, S.; DeGrado, W. F.; McCafferty, D. G.; Gai, F. Light-Induced Helix Formation. *J. Am. Chem. Soc.* **2002**, *124*, 12674–12675.

(32) Lednev, I. K.; Karnoup, A. S.; Sparrow, M. C.; Asher, S. A. α-Helix Peptide Folding and Unfolding Activation Barriers: A Nanosecond UV Resonance Raman Study. *J. Am. Chem. Soc.* **1999**, *121*, 8074–8086.

(33) Levy, Y.; Jortner, J.; Becker, O. M. Solvent Effects on the Energy Landscapes and Folding Kinetics of Polyalanine. *Proc. Natl. Acad. Sci. U.S.A.* **2001**, *98*, 2188–2193.

(34) Du, D.; Bunagan, M. R.; Gai, F. The Effect of Charge-Charge Interactions on the Kinetics of α-Helix Formation. *Biophys. J.* **2007**, *93*, 4076–4082.

(35) Mukherjee, S.; Chowdhury, P.; Bunagan, M. R.; Gai, F. Folding Kinetics of a Naturally Occurring Helical Peptide: Implication of the Folding Speed Limit of Helical Proteins. *J. Phys. Chem. B* **2008**, *112*, 9146–9150.

(36) Krejtschi, C.; Hauser, K. Stability and Folding Dynamics of Polyglutamic Acid. *Eur. Biophys. J.* **2011**, *40*, 673–685.

(37) Serrano, A. L.; Tucker, M. J.; Gai, F. Direct Assessment of the α-Helix Nucleation Time. *J. Phys. Chem. B* **2011**, *115*, 7472–7478.